

How consistent is the satellite derived SST-LHF relationship in comparison with observed values?

***P.M.Muraleedharan and T. Pankajakshan**
National Institute of Oceanography, Dona Paula, Goa 403 004, India
***murali@nio.org**

Abstract

Time series data for sea surface temperature (Moored Buoy), wind speed, air temperature, sea level pressure, relative humidity, short wave radiation and rainfall were collected close to the Lakshadweep islands for five months from July 2000 to cover two seasons viz; summer monsoon and autumn. Day and night passes of TMI data for the same period were analyzed to compare with the observed values. Daily mean values were then generated from both satellite-derived as well as observed parameters and daily latent heat flux (LHF) values computed using the advanced COARE-3.0 version of the model. In concurrence with earlier studies, the observed LHF-SST relationship was inverse as the SST during this season seldom fell below 27 °C. On the contrary the satellite derived LHF-SST relationship exhibited a direct correlation. It is also observed that the satellite underestimation of SST increases linearly on either side of a threshold value of 28.5 °C. Although the SST over the eastern Arabian Sea was generally above 27 °C, the satellite underestimation often produced SSTs less than 27 °C, thereby supporting a linear relationship with LHF as suggested by Zhang and McPhaden. Similarly for SSTs higher than 28 °C, the satellite underestimation prevented further decrease of LHF (to sustain the linear relationship) by virtue of the inverse relationship for SSTs higher than 28 °C. The overestimation of SST and WS in the satellite scenario generates a virtual enhancement of LHF values without cooling the sea surface. The linear relationship between SST and LHF is thus nothing but a virtual display of the observed inverse SST-LHF relationship.

Keywords : Validation, bias, Indian Ocean, latent heat flux, evaporation, humidity

1. Introduction

Accurate retrieval of air-sea exchange parameters from satellite is highly desirable as it contributes immensely to the climate studies. Due to the inherent difficulties in the direct flux measurement, indirect approaches to flux estimation have been widely adopted in spite of the large uncertainties associated with them. One of such approaches was the 'Bulk method' that is extensively used in numerical models and field applications. Blanc (1985) published his thorough and extensive review of the large differences among more than ten bulk flux algorithms. More recently Fairall *et al* (2003) have reported the final version of the bulk flux algorithm that emerged out of a carefully planned Coupled Ocean-Atmosphere Response Experiment (COARE) where more than 7216 hours of direct flux measurements were used to validate the bulk algorithm. They have succeeded in narrowing down the uncertainty from the then existing 20-30% level to 5% for wind speeds of 0-10 ms⁻¹ and to 10% for 10-20 ms⁻¹ wind speed. The remote sensing uncertainties would compound if the computations were based on data collected from satellite-mounted sensors. The algorithm was primarily based on data collected over the western Pacific warm pool and then extended to higher latitudes and in stronger winds to accommodate tropical and sub tropical climatic conditions.

Bhat (2003) has made an attempt to compute air sea fluxes over north Indian Ocean using Eddy Correlation and Inertial-dissipation methods (direct methods) to examine the validity of the widely used bulk algorithms (Zeng *et al.*, 1998) derived from TOGA_COARE data set. He has also compared the above LHF values with TOGA-COARE fluxes generated by Fairall *et al.*, (1996) and their results indicated good agreement between the fluxes from bulk and direct methods. Therefore in the present study the state of the art COARE_3.0 version of the algorithm is used for the surface flux estimation using both *in situ* and satellite data over the Eastern Arabian Sea, a unique basin with noticeable spatial and temporal variability in oceanographic and atmospheric parameters that governs the air-sea interaction processes (Prasannakumar *et al.*, 2001; Bhat, 2003; Madhuratap *et al.* 2003; Shankar *et al.*, 2004). Time evolution of satellite biases in latent heat flux (LHF) was analyzed during the summer monsoon and fall inter-monsoon seasons (autumn) and the reversal of bias during autumn is explained on the basis of similar reversal noticed for sea surface temperature (SST) and wind speed (WS) on either side of a certain threshold value of 28.5 °C and 5 ms⁻¹, respectively (Muraleedharan *et al.* 2006).

2. Data and Methodology

Time series data of SST, WS, water vapor, air temperature, relative humidity, incoming solar radiation, sea level pressure and daily rainfall were obtained from a set of island-based (Autonomous Weather Station and rain gauge) and ocean-based platforms (moored buoy) located very close to each other (10.5° N; 72° E) for a period of five months from July 2000 to cover the southwest monsoon (Jul – Sep) and autumn (Oct – Nov) seasons (Fig.1). Continuous data were not available beyond this period. The data collection facilities were established as a part of Indian Remote Sensing Satellite (IRS-P4) validation mission. Validation results indicated that the land contamination was minimum in the microwave bands as the island is only about 5 km² in area and is situated more than 350 km away from the mainland (Muraleedharan et al., 2004). Using half-hourly surface meteorological data, 3-hourly SST data and daily rainfall estimates, daily fields were constructed to compute LHF using COARE_3.0 scheme. Ascending and descending passes of TRMM (Tropical Rainfall Measuring Mission) Microwave Imager (TMI) data were then analyzed for SST, WS and WV to prepare collocated data points. Surface level specific humidity (q_a) was derived from WV using the Liu and Niiler (1984) model. Retrieval of air temperature (T_a) was carried out using polynomials constructed between q_a and T_a by partitioning the northern Indian Ocean into several temporal and spatial grids to accommodate large variation of T_a . Such partitioning would bring down the root mean square (RMS) error to an acceptable limit of 1 °C (Sathe and Muraleedharan, 1999). Liu (1984) showed that a large portion of the water vapor is concentrated in the atmospheric boundary layer. The vertical distribution of water vapor varies with diurnal and synoptic fluctuations of the boundary layer at time-scale shorter than a month. With this assumption the model computes monthly mean fields of surface humidity from monthly mean integrated water vapor derived from satellite. In order to justify the present computations for shorter time intervals, LHF from both satellite and observed values were computed (using the same model) for various time averaging periods viz; monthly, weekly, 3 day average, daily and instantaneous (Table 1). The daily comparisons made here is statistically significant and hence justifiable. COARE_3.0 program computes LHF from the above inputs by assuming a constant pressure of 1008 mb and a “no rainfall” condition. Pressure variations noticed in conventional surface level data contributed

insignificant changes in the LHF calculation. Turbulent LHF computed in the COARE_3.0 program is independent of the rainfall effect (Fairall *et al.*, 2003) and hence the above assumption makes no difference while comparing with *in situ* LHF estimate. For the purpose of comparison heat flux due to rainfall was separately calculated in the program. Moreover, the intense rainfall events ($> 1 \text{ mm hr}^{-1}$) that contributed significant variation in air sea heat flux exchange were very few (less than 20% of the sampling period) even in peak monsoon months.

3. Results and Discussion

The Arabian Sea is a unique tropical basin as it experiences extreme seasonal variabilities in oceanographic and atmospheric processes due to its peculiar geographic location (Prasannakumar *et al.*, 2000 & 2001). Temporal and spatial variability of geophysical parameters occurring at the interface is large enough to make this basin an experimental laboratory. The monsoonal reversal of remote sensing bias in LHF over the eastern Arabian Sea further demonstrates the complexity of this basin (Muraleedharan *et al.*, 2006). Figure 2 illustrates time series data of WS, SST, T_a , Relative humidity (RH) and sea level pressure from July to November 2000. In general, high WS of $6\text{-}10 \text{ ms}^{-1}$ during summer and $< 4 \text{ ms}^{-1}$ during autumn prevailed over this area. Sea surface temperature was marginally warmer than T_a during summer ($\sim 28 \text{ }^\circ\text{C}$) but the difference peaked in autumn when the SST shot to $30 \text{ }^\circ\text{C}$. Relative humidity also indicated a similar reversing trend from summer to autumn but the trend was a mirror reflection of T_a . Sea level pressures did not show any seasonal trends and rather roughly follow 1008 mb pressure level throughout the period of investigation. The data were free from random errors as such offshoots had been discarded in the initial stages of the data analysis.

The observed air-sea interaction parameters such as SST, WS and humidity were analyzed in detail along with the derived LHF to facilitate comparison with parameters and products derived from satellite. The statistics of relationship between *in situ* and satellite products during the period of investigation are listed in Table 2. All the relationships were found to be statistically significant to 95% level. The bias (satellite – *in situ*) appeared to be negative for both SST and humidity gradient (D_q) while it was positive for WS. Reversal of LHF bias was noticed in autumn. A closer look revealed that the SST bias during autumn was three times the bias noticed

in summer while WS and humidity biases remained more or less unchanged. The SST bias had therefore a major role in modifying (reversing) the LHF bias during autumn.

Relationships between various parameters responsible for air-sea exchange of fluxes are illustrated in figures 3&4 for both observed and satellite derived products. It is quite natural that the relationship, in general, resembled one another in the left and right panels except that of SST and D_q with LHF where the mean trend appears to be opposite (Figs. 3 a&b and e&f). The reason for such an unconventional trend is worth investigating.

3.1. Reasons for the reversal of relationship between SST and LHF

Scatter plots of *in situ* SST and LHF exhibited inverse trend (Figs. 3e) as the SST seldom dropped below 27 °C over this region during summer and autumn (Sui *et al.*, 1991; Ramnathan and Collins, 1992; Zhang and McPhaden, 1995) but the synchronized satellite measurements showed a direct relationship between SST and LHF with comparable coefficient of correlation (Fig. 3f). Although the SST-LHF relationship was direct for satellite products, the scatter between SSTs 27.5 °C and 29.5 °C did indicate an inverse pattern. The points below 28 °C and above 29 °C were instrumental in reversing the trend. This peculiar behavior of observed and satellite values is explained on the basis of the results of Zhang and McPhaden (1995) and Muraleedharan *et al* (2006). Zhang and McPhaden (1995) showed that the LHF increases with SST for SSTs below 27.5 °C, consistent with thermodynamic considerations. However, at SSTs above 27.5 °C, LHF decreases with increasing SST as a result of dynamic interaction between the large-scale circulation and SST. When SST is high, the atmosphere becomes more convectively unstable. The resultant interaction between convection and large-scale circulation enhances the large-scale low-level convergence by mass continuity. In the center of the low-level convergence the wind speed is low, yielding low LHF. Figure 5, reproduced from Muraleedharan *et al.*, (2006), has established (on the basis of the mean trend of the best fit of the scatter) that the satellite-sea truth bias (residual) is minimum for SSTs close to 28.5 °C and that it increases progressively on either side of this threshold. In other words, satellite underestimates colder (< 28.5 °C) and warmer (> 28.5 °C) SSTs and the process of underestimation progressively increases on either side the above threshold. The lower SST values below 27.5 °C

in Fig. 3f are an underestimation of the values falling just above 27.5 °C in Fig. 3e. As these values fall below 27.5 °C, they have a direct relationship with LHF (Fig. 3f) as shown by Zhang and McPhaden (1995). The relationship reverses for SSTs higher than 27.5 °C and the nature of the scatter between 27.5 and 29.5 °C in Fig.3f indicates an inverse pattern. The scatter towards higher SST (> 29 °C), however, could not be explained solely on the basis of the inverse relationship shown by Zhang and McPhaden (1995). The underestimation of SST above 28.5 °C (Muraleedharan *et al.*, 2006) supports high LHF through inverse relationship (Zhang and McPhaden (1995) thereby initiating the reversing trend of the relationship (Fig. 3f). The few positive residuals in Fig. 5c indicate overestimation of SST by satellite and such overestimation is instrumental in reversing the SST-LHF relationship.

In order to understand the nature of scatter obtained in Fig 3f , contours of LHF, WS and D_q were plotted with SST on the x - axis and SST- residuals on the y - axis (Fig.6). Similar plots were constructed for both *in situ* and satellite data products to facilitate comparison (Fig.6, left and right panels, respectively). From the figures (Figs.6 a, c & e) it is evident that the high LHF values (> 120 Wm^{-2}) are associated with high WS (> 5 ms^{-1}), low SST (< 28.5 °C) and low D_q values (< 7.5 $g\ kg^{-1}$) and such conditions prevail over the eastern Arabian Sea during summer monsoon. Similarly, low winds (< 5 ms^{-1}), high SST (> 28 °C) and high humidity gradient (> 8 $g\ kg^{-1}$) in the same figure represent fall inter-monsoon season. The presence of relatively high LHF (> 100 Wm^{-2}) in association with low wind speeds (< 5 ms^{-1}) and high SSTs (> 29.5 °C) unambiguously explains the role of humidity gradient in overcoming the inverse effect of SST on LHF (Figs. 6 a, c & e). Interestingly, the highest LHF values are generated by a combination of WS, SST and D_q values that were closer to the respective thresholds (28.5 °C; 5 ms^{-1} ; 8 $g\ kg^{-1}$) reported earlier (Muraleedharan *et al.*, 2006). In brief, the thresholds appear to be the optimum levels to produce maximum LHF over this part of the ocean. However, the residuals corresponding to high LHF values indicated that the satellite overestimates SST and WS by approximately 1 °C and 2 ms^{-1} , respectively and underestimates humidity gradient by 2 $g\ kg^{-1}$ (Figs. 6 b, d & f). The process of underestimation of SST below 28.5 °C, therefore, induces high LHF by invoking the thumb rule proposed by Zhang and McPhaden (1995), thereby exhibiting a linear relationship of SST with LHF. On the other hand, in the remote sensing scenario, the effect of low SST and low humidity gradient overcomes the effect of relatively high WS

(associated with low SST) to generate relatively low LHF values (Figs. 6 *b*, *d* & *f*). The underestimated SST therefore has a direct relationship with LHF in the satellite scenario. The overestimation of SST associated with high LHF (Fig.6*a*) along with the overestimation of WS (Fig.6*c*) would lead to virtual enhancement of evaporation (LHF) and hence the relationship fails to follow the thumb rule of Zhang and McPhaden (1995) where the enhanced LHF is expected to cool the underlying ocean. The linear relationship between satellite derived SST and LHF is, therefore, a virtual display of the inverse relationship obtained from the *in situ* measurements.

4. Concluding Remarks

Latent heat fluxes were estimated from both in situ and satellite based parameters after averaging them to daily values. The statistical comparison between satellite and in situ observation indicated negative biases for both SST and D_q and a positive bias for WS. The negative LHF bias during summer is reversed to positive bias in autumn. The seasonal variation of bias is very conspicuous for SST and hence is instrumental in reversing the LHF during autumn (Table 1). Subsequently the SST-LHF relationships were examined for both in situ and satellite based measurements. An inverse relationship is noticed between SST and LHF for in situ observation and the relationship reverses for satellite-based computations (Figs. 3 *e&f*).

The inverse trend observed for in situ data is in accordance with earlier observations and also due to the fact that SST seldom dropped below 27 °C over this region during summer and autumn. According to Muraleedharan et al., (2006) satellite underestimate colder (< 28.5 °C) and warmer (> 28.5 °C) SSTs and the process progressively increases on either side of the above threshold. SSTs falling below and above 27.5 °C have direct and inverse relationships with LHF respectively (Zhang and Mc Phaden,1995). The nature of scatter between 27.5 °C and 29.5 °C in Fig. 3*f* indicates an inverse pattern. The underestimation of SST above 28.5 °C (Muraleedharan et al., 2006) supports high LHF through inverse relationship (Zhang and McPhaden (1995). This would reverse the trend of the scatter to a direct relationship. Few overestimation of SST noticed in Fig.5*c* would also compound to the above direct relationship.

The contours of LHF, WS and D_q plotted against SST explains the interrelationship of these parameters during two contrasting seasons. High LHF (> 120 Wm²) are associated with high WS (> 5 ms⁻¹), low SST (< 28.5 °C) and low D_q values (< 7.5 g kg⁻¹) during monsoon

period. Relatively high LHF ($>100 \text{ Wm}^{-2}$) in association with low WS ($< 5 \text{ ms}^{-1}$), high SST ($> 28.5 \text{ }^\circ\text{C}$) and high D_q ($> 8 \text{ g kg}^{-1}$) explains the role of D_q in overcoming the inverse effect of SST on LHF during autumn. In brief the thresholds reported (Muraleedharan et al, 2006) are the optimum levels to produce maximum LHF values over this basin. But in the satellite scenario, the overestimation of SST associated with high LHF along with the overestimation of WS would lead to virtual enhancement of evaporation (LHF) and hence the relationship fails to follow the thumb rule of Zhang and McPhaden (1995) where the enhanced evaporation is expected to cool the underlying ocean. Hence the linear relationship obtained between SST and LHF is a virtual display of the inverse relationship obtained from field observation.

The direct and inverse SST-LHF relationship on either side of a threshold SST (Zhang and McPhaden, 1995) explains the natural control exerted by SST on LHF exchange. Muraleedharan et al., (2006) has shown similar SST threshold ($28.5 \text{ }^\circ\text{C}$) and the satellite bias tend to increase on either side. Wind speed bias has also shown decreasing trend on either side of a threshold (5ms^{-1}). The corresponding threshold for D_q is 8 g kg^{-1} . It is observed that the optimum production of LHF occurs over eastern Arabian Sea when these conditions are met. The above thresholds in the Arabian Sea demarcate two seasons representing extreme climatic conditions. The negative satellite bias during monsoon season decreases when SST increases over Arabian Sea. However during autumn, the negative bias increases when SST increases. The residuals corresponding to high LHF values (threshold points) indicated that the satellite overestimate SST and WS by $1 \text{ }^\circ\text{C}$ and 2 ms^{-1} respectively and underestimates D_q by 2 g kg^{-1} . The selective overestimation and underestimation of the above surface meteorological parameters with respect to the above threshold points make the validation process more complex over this part of the ocean. Since validation is an integral part of any satellite mission, proper understanding of the variability of the parameters (to be validated) with time and space is essential. Arabian Sea is known for large temporal and spatial variability of surface meteorological parameters, which are now measured from satellite. Long-term observational platforms for measuring all parameters are yet to be established over this basin to monitor the ocean atmosphere interaction. In view of the large temporal and spatial variability of Arabian Sea, several such platforms to represent all weather conditions are essential to derive useful information from validation experiments. Such efforts would fetch information to develop regional models to predict reasonably accurate geophysical parameters.

Acknowledgements: We thank the Director, National Institute of Oceanography, Goa and The Director, Space Application Center, Ahmedabad for the facilities and funds to set up the Autonomous Weather Station at Lakshadweep Island. The efforts of Dr. Ismail Koya, Deputy Director, Science and Technology, Kavarathi, in collecting surface meteorological data are gratefully acknowledged. We also thank Dr. Frank Wentz and his office 'Remote Sensing Systems' for providing SSMI and TMI products. This is NIO contribution number 4288.

References:

- Bhat, G.S., 2003, Measurement of Air Sea fluxes over the Indian Ocean and the Bay of Bengal, *Journal of Climate*, 16, pp. 767 – 775.
- Blanc, T.V., 1985, Variation of bulk-derived surface flux, stability and roughness results due to the use of different transfer coefficient schemes, *Journal of Physical Oceanography*, 15, pp. 650 - 669.
- Fairall, C.W., Bradley, E.F., Progers, D., Edson, J.B., and Young, G.S., (1996). Bulk parameterization of air-sea fluxes for tropical ocean Global Atmosphere Coupled Ocean-Atmosphere Response Experiment. *J. Geophys. Res.*, 101, 155 – 192.
- Fairall, C.W., Bradley, E.R., Hare, J.E. Grachev, A.A., and Edson, J.B., 2003, Bulk Parameterization of Air-Sea Fluxes: Updates and verification for the COARE Algorithm, *Journal of Climate*, 16, pp. 571 – 591.
- Liu, W.T. (1984). Estimation of latent heat flux with SEASAT-SMMR, a case study in N. Atlantic. *Large-Scale Oceanographic Experiments and Satellites*, C.Gautier and M. Fieux, Eds., Reidel.
- Liu, W.T. and Niiler, P.P., 1984, Determination of monthly mean humidity in the atmospheric surface layer over ocean from satellite data, *Journal of Physical Oceanography*, 14, pp. 1451-1457.
- Madhupratap, M, Mangesh Gauns, Ramaiah, N., Prasanna Kumar, S., Muraleedharan, P.M., De Sousa, S.N., Sardessai, S., and Usha Muraleedharan, 2003, Biogeochemistry of the Bay of Bengal: physical, chemical and primary productivity characteristics of the central and western Bay of Bengal during summer monsoon 2001, *Deep Sea Res. II*, 50, pp. 881 – 896.

- Muraleedharan, P.M., Pankajakshan, T., and Harikrishnan, M., 2004, Validation of Multi-channel Scanning Microwave Radiometer on-board Oceansat-I, *Current Science*, 87, pp. 370 - 376.
- Muraleedharan, P.M., Pankajakshan, T., Sathe, P.V., Murty, V.S.N., and Santosh, K.R., 2006, Monsoonal Reversal of Remote Sensing Biases in Latent Heat Flux over the Eastern Arabian Sea, *Geophysical Research Letters*, 33, No. 18, L18605, September, 2006..
- Prasanna Kumar, S., Madhupratap, M., Dileep Kumar, M., Gauns, M., Muraleedharan, P.M., Sarma, V.V.S.S., and De Souza, S.N., 2000, Physical control of primary productivity on a seasonal scale in central and eastern Arabian Sea, *Proceedings of Indian Academy of Sciences*, 109, pp. 433 – 441.
- Prasanna Kumar, S., Ramaiah, N., Mangesh Gauns, Sarma, V.V.S.S., Muraleedharan, P.M., Raghukumar, S., Dileep Kumar, M., and Madhupratap, M., 2001, Physical forcing of biological productivity in the Northern Arabian Sea during the Northeast Monsoon. *Deep Sea Res. II*, 48, pp. 1115 – 1126.
- Ramanathan, V. and Collins, W., 1992, Thermostat and global warming, *Nature*, 357, pp. 649.
- Sathe, P.V., and Muraleedharan, P.M., 1999, Retrieval of sea surface air temperature from Satellite data over Indian Ocean: An empirical approach, *Asian Meteorological Online Newsletter*, Vol. 3, No.1
- Shankar, D., Gopalakrishna, V.V., Shenoi, S.S.C., Durand, F., Shetye, S.R., Rajan, C.K., Johnson, Z., Araligidad, N., and Michael, G.S., 2004, Observational evidence for westward propagation of temperature inversions in the southeastern Arabian Sea, *Geophysical. Research Letters*, 31, No. 8, L08305, April, 2004..
- Sui, C,-H., Lau, K,-M., and Betts, A.K., 1991, An equilibrium model for the coupled ocean-atmosphere boundary layer in the Tropics, *Journal of Geophysical Research*, 96, pp. 3151 – 3163.
- Zeng, Xubin, M. Zhao and R.E. Dickinson, (1998). Inter comparison of Bulk Aerodynamic Algorithms for the computation of sea surface Fluxes using TOAGA COARE and TAO Data. *J. Climate.*, 11, 2628 – 2644.
- Zhang, G.J., and McPhaden, M.J., 1995, The relationship between Sea Surface Temperature and Latent Heat Flux in the Equatorial Pacific, *Journal of Climate*, 8, pp. 589 – 605.

Table 1. Results of comparison between in situ and satellite based LHF computation from monthly to shorter time averaging periods

Averaging Periods	Statistical Analysis							
	No. of Matches ' <i>n</i> '		RMSD		Correlation Coefficient ' <i>R</i> '		Bias	
	Summer	autumn	Summer	autumn	Summer	autumn	Summer	autumn
Instantaneous	44	24	26	36	0.78	0.69	4	21
Daily	79	56	27	40	0.75	0.44	-10	23
3day	75	56	23	30	0.79	0.42	-12	20
Weekly	67	56	21	22	0.81	0.52	-15	17
Monthly	50	56	21	13	0.93	0.14	-21	10

Parameter	Statistics	Summer <i>n</i> = 79	Autumn <i>n</i> = 56	Summer & Autumn, <i>n</i> = 135
Sea Surface Temperature	<i>R</i>	0.79	0.66	0.80
	bias	- 0.10	- 0.30	- 0.19
Wind Speed	<i>R</i>	0.88	0.75	0.88
	bias	1.82	1.72	1.77
Humidity gradient	<i>R</i>	0.71	0.79	0.84
	bias	- 3.00	- 3.00	- 3.00
Latent Heat Flux	<i>R</i>	0.73	0.48	0.62
	bias	- 9.00	13.60	0.43

Table 2 Statistical relationships between *in situ* and satellite derived products during Summer, Autumn and the entire period. '*n*' denotes number of data points and '*R*' the correlation coefficient.

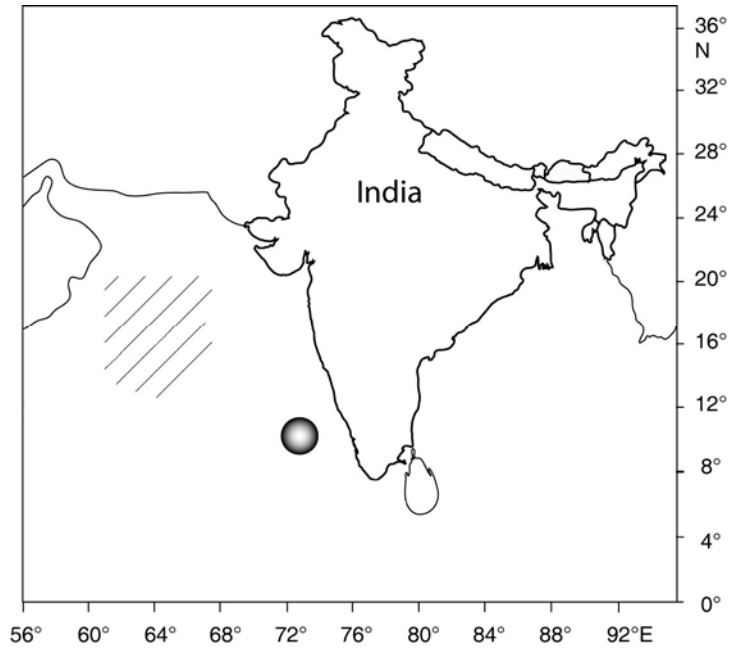


Fig.1. Map showing the location (denoted by the circle) of the observational platforms.

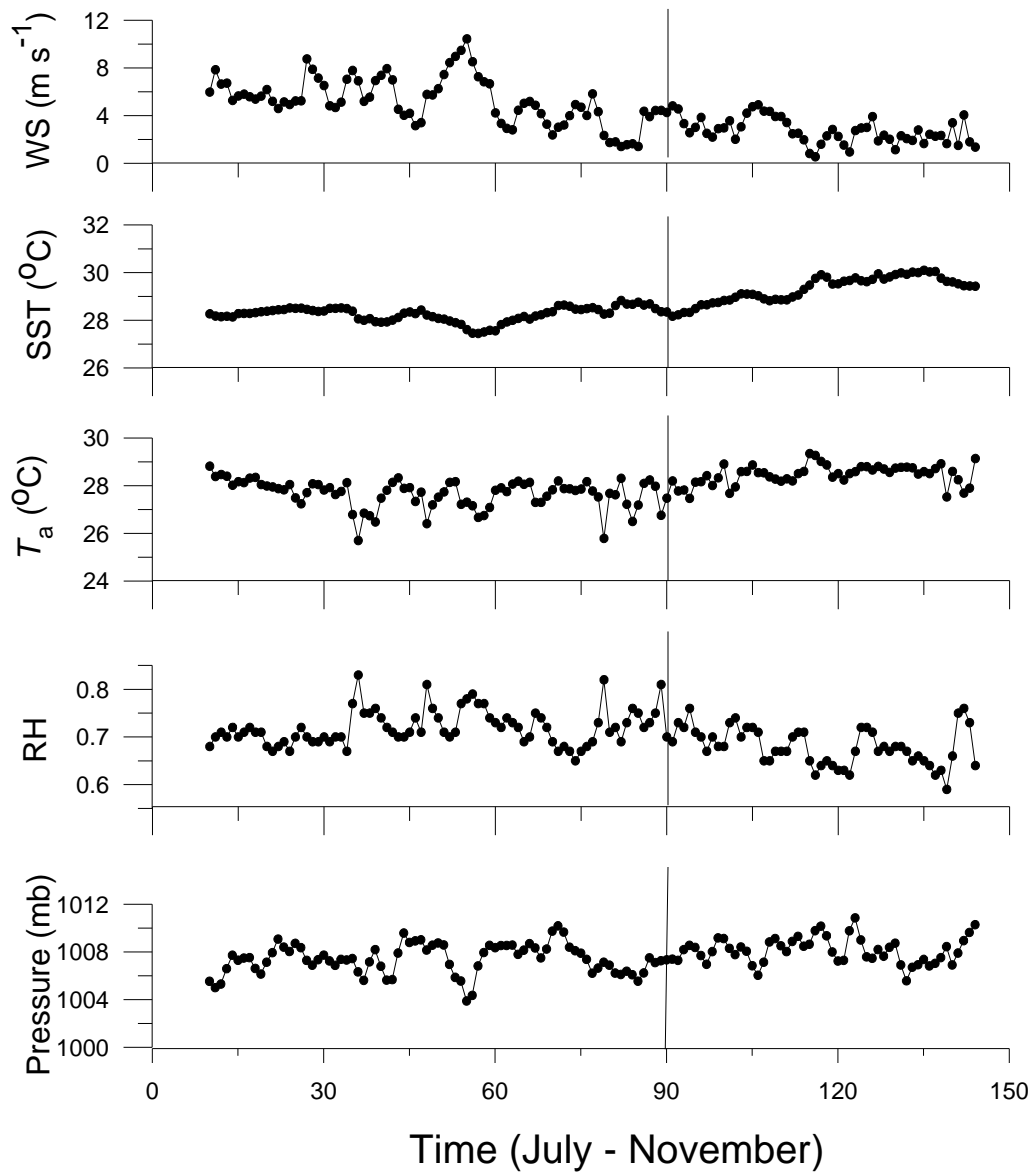


Fig. 2. Time series measurement of WS, SST, T_a , RH and pressure during monsoon (July – September) and autumn (October – November). The vertical line demarcates monsoon and autumn.

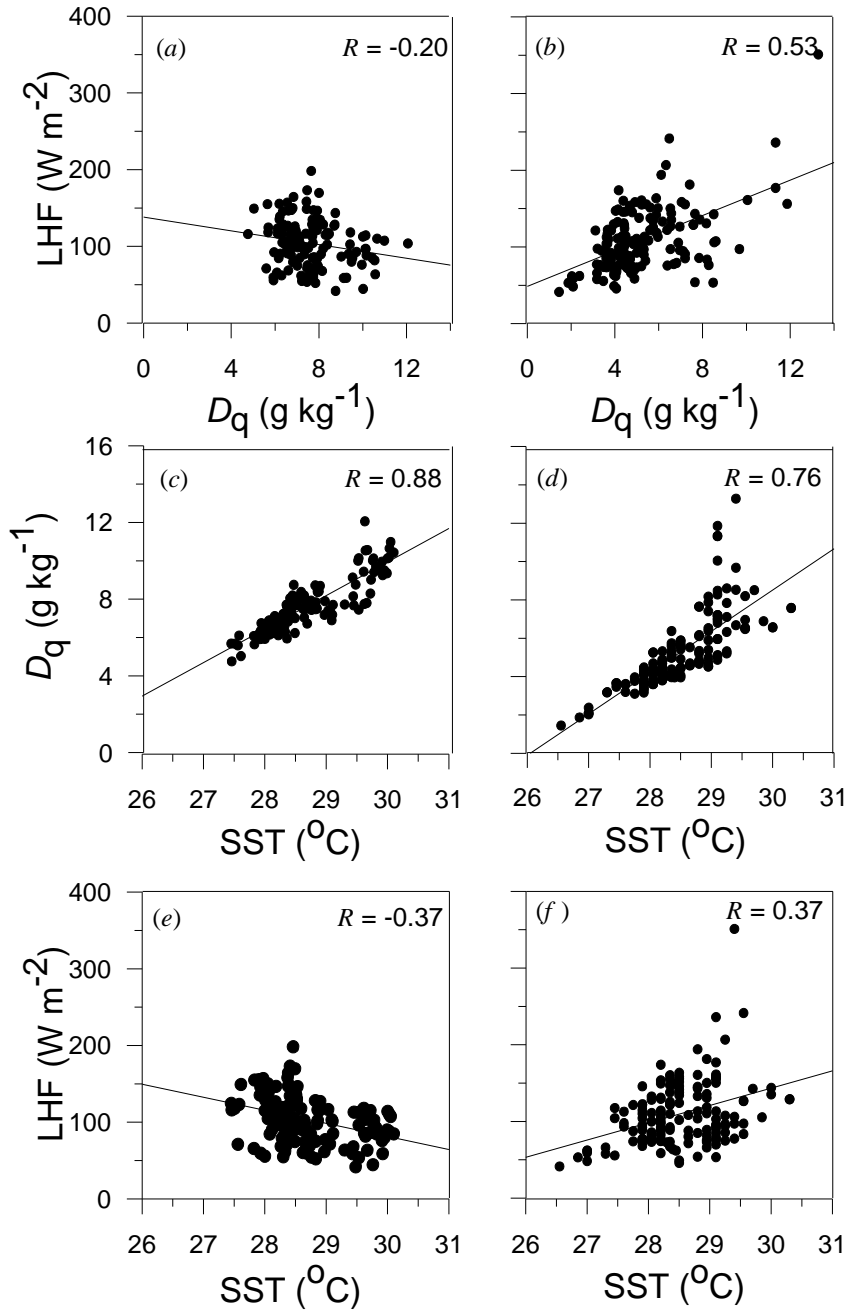


Fig. 3. Scatter diagram of observed (left panel) vs satellite derived (right panel) parameters.

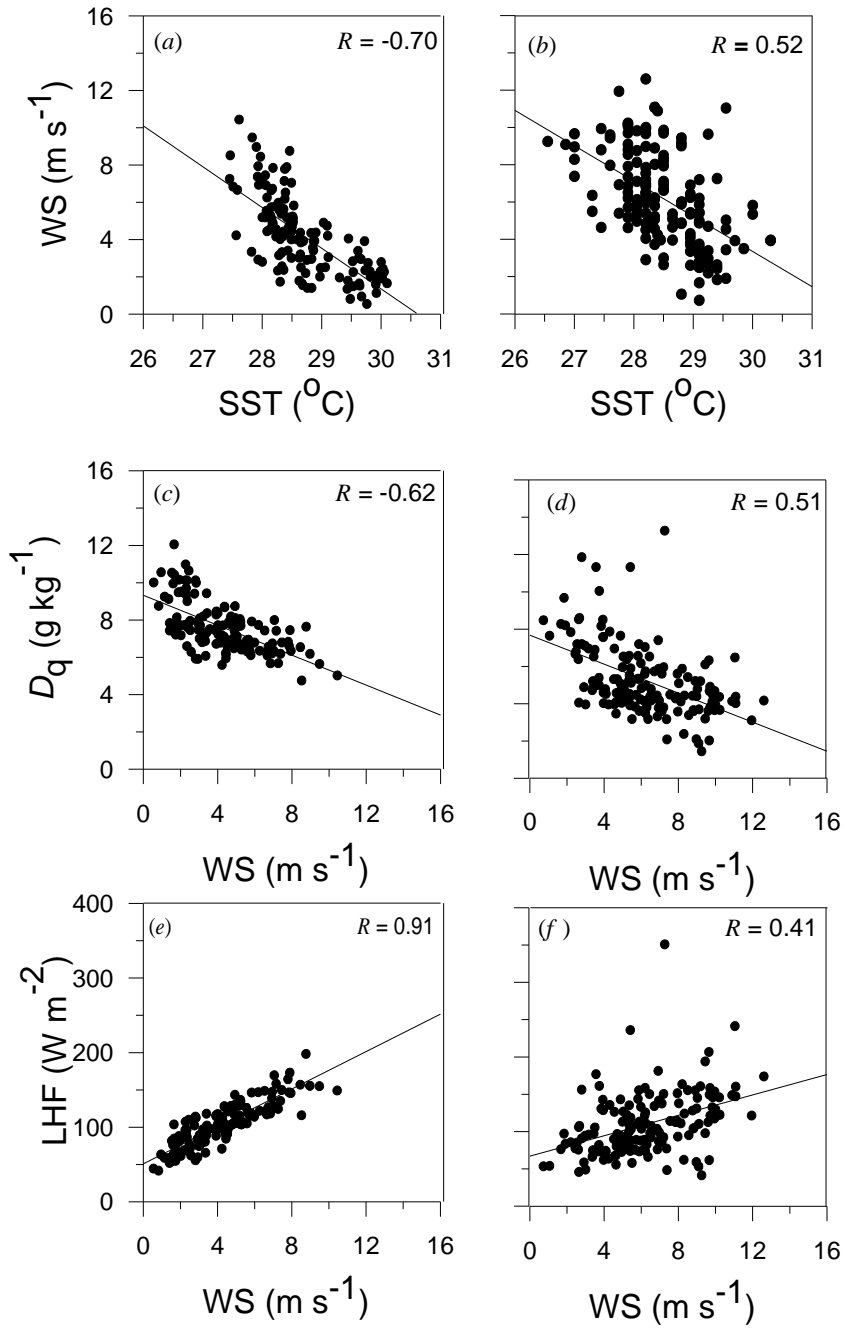


Fig. 4. Scatter diagram of observed (left panel) vs satellite derived (right panel) parameter.

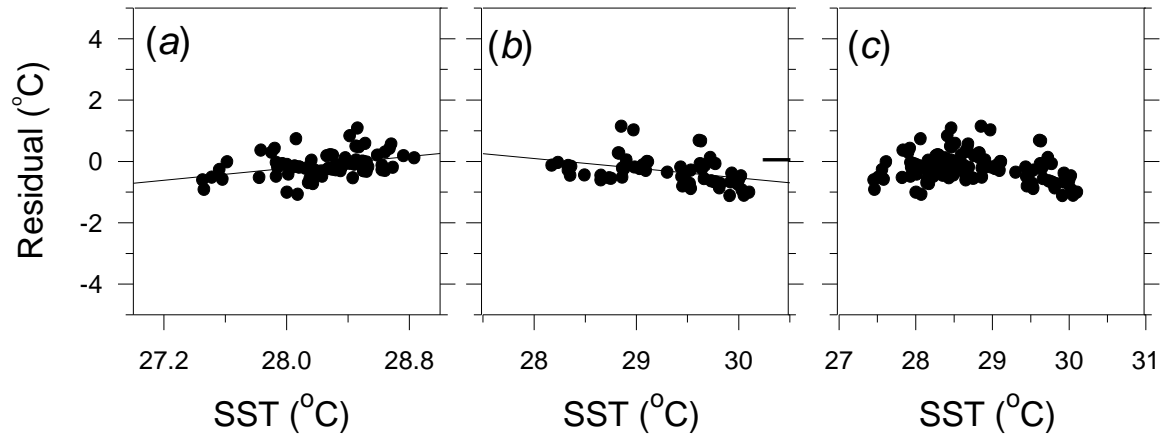


Fig. 5. Residuals (Satellite – Observed) vs observed SST during summer when $SST < 29\text{ }^{\circ}\text{C}$ (a), during autumn when $SST > 28\text{ }^{\circ}\text{C}$ (b) and for both situations (c). (Muraleedharan *et. al.*, 2006)

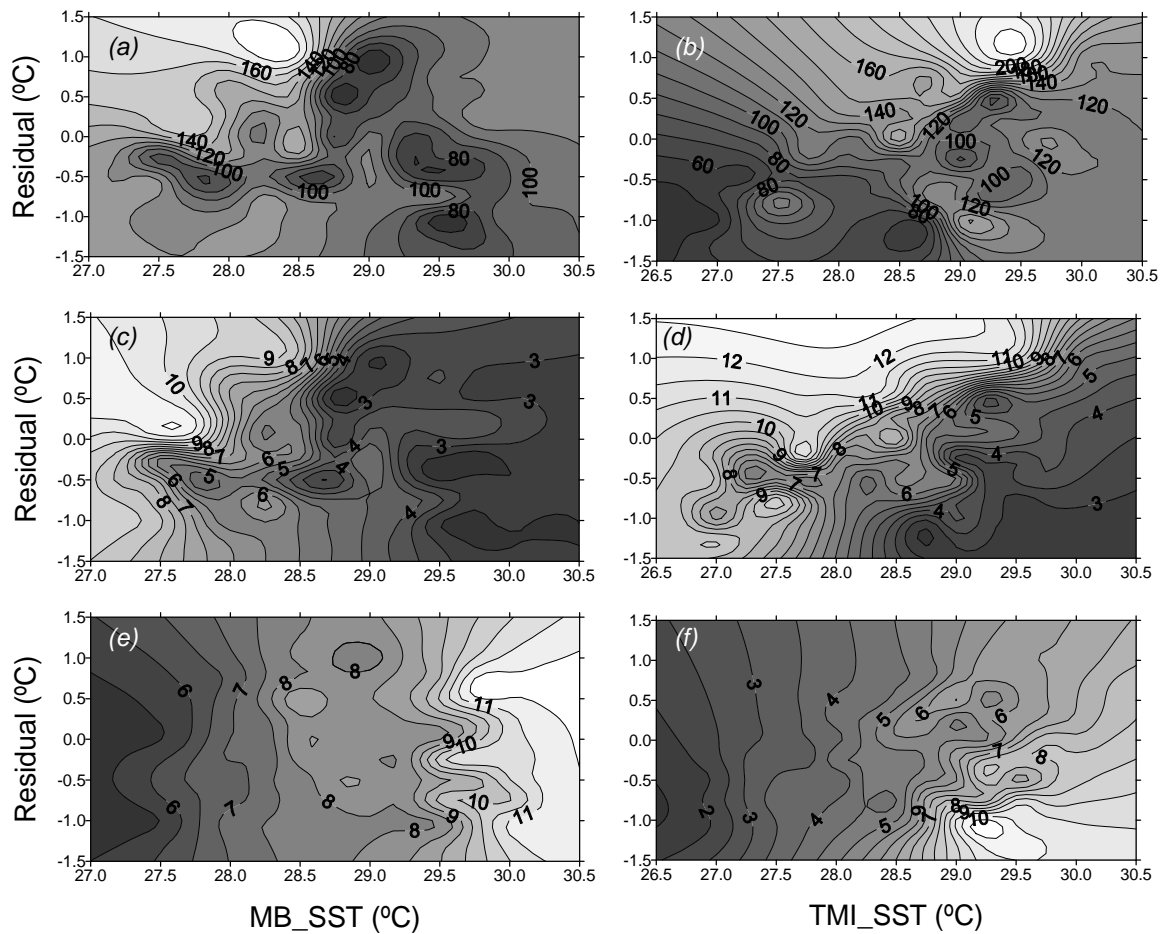


Fig.6. Contours of LHF (Wm^{-2}) (top panels), WS (ms^{-1}) (middle panels) and humidity gradient (g kg^{-1}) (bottom panels) plotted against SST and SST-residual for *in situ* (Moored Buoy - MB) (left panels) and satellite derived [TRMM (Tropical Rainfall Measuring Mission) Microwave Imager-TMI] (right panels) products.